Journal of Nuclear Materials 378 (2008) 180–187

Contents lists available at ScienceDirect

Journal of Nuclear Materials

journal homepage: www.elsevier.com/locate/jnucmat

Lanthanum carbide-based porous materials from carburization of lanthanum oxide and lanthanum oxalate mixtures

L. Biasetto [a,b,*], P. Zanonato [c], S. Carturan [b], P. Di Bernardo [c], P. Colombo [a,d], A. Andrighetto [b], G. Prete [b]

[a] Università di Padova, Dipartimento di Ingegneria Meccanica, Via Marzolo 9, 35131 Padova, Italy
[b] INFN-Laboratori Nazionali di Legnaro, V.le dell'Università 2, 35020 Legnaro (PD), Italy
[c] Università di Padova, Dipartimento di Scienze Chimiche, Via Marzolo 1, 35131 Padova, Italy
[d] Department of Materials Science and Engineering, The Pennsylvania State University, University Park, PA 16802, USA

ARTICLE INFO

Article history:
Received 23 April 2008
Accepted 4 June 2008

ABSTRACT

Porous lanthanum carbide (LaC_2) based materials were prepared from lanthanum oxalate ($La_2(C_2O_4)_3$), lanthanum oxide (La_2O_3) and graphite mixtures. The molar ratio between La_2O_3 and $La_2(C_2O_4)_3$ was varied in order to detect the effect of starting mixtures on the porosity of the products. Samples structure and morphology were investigated by means of scanning electron microscopy, equipped with the probe for elemental analysis, (SEM-EDS) and X-ray diffraction spectrometry (XRD). As for the porosity characterization, the amount of total porosity was derived from the comparison between the theoretical and the measured density values, whereas a thorough investigation on the amount of open porosity and pore size distribution was carried out by means of Mercury Intrusion Porosimetry, after carburization and sintering. Emissivity measurements were performed upon carburization and sintering in order to verify the effect of porosity on emissivity values.

1. Introduction

Facilities that make use of isotope separator on-line (ISOL) for the production of radioactive ion beams (RIB) are gaining significant interest worldwide, mainly because they offer unique opportunities to further extend our knowledge about the structure of the atomic nucleus, the formation processes of the stars and of the heavy-elements [1]. Many facilities have been built worldwide in the last decade (i.e. HRIBF at ORNL, ISOLDE at CERN, TRIUMF) and new ones are currently under development. Within this context, the SPES facility at LNL-INFN is now under development. This ISOL facility will produce 10^{13} fissions/s by means of a 40 MeV proton beam and a current of 0.2 mA directly impinging on uranium carbide thin (≈1 mm) disks [2,3]. Isotopes will be produced by means of fission nuclear reactions occurring in the disks.

Even though the above mentioned facilities differ from each other for several aspects, they have a common point of interest related to the optimization of target yield, which is a function both of the flux of injector and of the product cross section, number of target nuclei per unit area, and release efficiency. This last point is very tricky, since release efficiency depends on the diffusion of isotopes within the target and effusion of isotopes towards the ionization source which, in turn, are strictly dependent on target characteristics such as composition, crystalline structure, morphology (grain size, amount and size of porosity). In order to decrease the release time, the targets have to be uniformly heated at temperatures ranging between 1500 °C and 2200 °C under vacuum. Appropriate operating temperatures must be chosen each time depending on the target chemical, thermal, and mechanical properties.

In order to design the best target it is necessary to consider, besides cross section and diffusion coefficient, properties such as:

1. The target limiting temperature, defined as the temperature at which the vapor pressure of the target materials begins to deleteriously affect the ionization efficiency of the particular ion source used in the RIB generation process.
2. The target emissivity and thermal conductivity, responsible for heat dissipation during the target bombardment. High emissivity and thermal conductivity grant for good heat dissipation of the target and prevent its overheating.
3. The target density and permeability. The presence of open porosity favors both diffusion and permeability [4]. The presence of low density species (such as carbon) reduces the overall density of the component, thus allowing faster release times. Fast diffusion and effusion of the isotopes are necessary in order to prevent their condensation on the cold target regions and their decay before reaching the ion source.

From all the above mentioned reasons, it is clear that the target composition and morphology play a key role in the design of the primary ion source for the facility.

* Corresponding author. Address: Università di Padova, Dipartimento di Ingegneria Meccanica, Via Marzolo 9, 35131 Padova, Italy.
E-mail address: lisa.biasetto@lnl.infn.it (L. Biasetto).

0022-3115/$ - see front matter © 2008 Elsevier B.V. All rights reserved.
doi:10.1016/j.jnucmat.2008.06.016

Among the possible choices for the materials constituting the target, low density, carbon dispersed metal carbides (MC_x) are quite promising. In particular, uranium and thorium dicarbides (UC_2 and ThC_2), that show very high-limiting temperature values (2100 °C and 2650 °C, for U- and Th-carbide, respectively [5]), seem to be the ideal candidates [5–7]. They can be produced in situ by reaction of a precursor (metal or metal oxide powder) with carbon (graphite powder or other carbon precursors forming a low density foam) according to Eqs. (1) and (2),

$$M + 2C + nC \rightarrow MC_2 + nC \quad (1)$$

$$MO_2 + 4C + nC \rightarrow MC_2 + 2CO + nC \quad (2)$$

where nC represents the excess of carbon necessary for the dispersion of the metal carbide in graphite.

The CO release during carbothermal reduction is responsible for the formation of pores. However the sintering processes, which take place at higher temperatures than the carbothermal reduction, can cause pores of small dimension to collapse if the sintering is not carried out in appropriate conditions. This shortcoming makes very difficult to properly control the amount of porosity generated upon carbothermal reduction.

Previous attempts for the production of porous uranium carbide used the carbothermal reduction of uranium oxide or an interconnected matrix (fibrous SiC, graphite cloth or reticulated vitreous carbon) as a support for a thin film of a suitable uranium carbide, obtained by the paint coating technique [8]. Recently, the usage of lanthanum dicarbide (LaC_2) was suggested as a substitute of uranium and thorium compounds for preliminary bench tests on the production and characterization of highly porous carbides [9,10]. In [9], a first attempt to develop porosity by using lanthanum oxalate was reported. In this work, a systematic study on the effects of changes of the starting mixtures (lanthanum oxalate/lanthanum oxide) on the final material characteristics (emissivity, degree of sintering, porosity amount and pore size, and interconnectivity of the pores) is presented.

2. Experimental

Porous lanthanum carbide–graphite samples were prepared by means of carbothermal reduction of lanthanum oxide (La_2O_3), lanthanum oxalate ($La_2(C_2O_4)_3$) and graphite mixtures. In the generic case of a molar ratio oxide/oxalate = x/y, the carbothermal reaction can be represented by Eq. (3)

$$xLa_2O_3 + yLa_2(C_2O_4)_3 + (11x + 14y)C \rightarrow 2(x + y)LaC_2 + (4x + 7y)C + (3x + 6y)CO\uparrow + 3yCO_2\uparrow \quad (3)$$

$$La_2(C_2O_4)_3 + 14C \rightarrow 2LaC_2 + 7C + 6CO\uparrow + 3CO_2\uparrow \quad (4)$$

$$La_2O_3 + 11C \rightarrow 2LaC_2 + 4C + 3CO\uparrow \quad (5)$$

In its final form, Eq. (3) is the sum of Eqs. (4) and (5) which takes into account that at about 700 °C (and well below carburization) $La_2(C_2O_4)_3$ is first completely converted to La_2O_3 (with CO and CO_2 release) [11], and only in a successive step the carbothermal reaction occurs between as received La_2O_3, La_2O_3 deriving from the decomposition of oxalate and graphite, with CO release. In order to detect the effect of lanthanum oxalate on the porosity of the final material, samples with different lanthanum oxide/lanthanum oxalate molar ratios were prepared. In Table 1 an overview of the mixtures employed is reported.

The La_2O_3 and C powders were purchased from Sigma–Aldrich and used as received. Lanthanum oxalate powders were dried under vacuum at 250 °C for 3 h, before mixing (Table 2).

The labeling scheme reported in Table 1 indicates the relative molar amounts of lanthanum oxide (LO) and lanthanum oxalate (LOx) in the samples. For all the samples, 2 wt% of phenolic resin (10 wt% solution in acetone) was added as a binder. Careful mixing of the powders and cold-pressing for 60 min with a pressure of 750 MPa afforded disks of 13 mm diameter and approximately 1 mm thickness. The green pellets were heat treated under vacuum (1×10^{-4} Pa) in a dedicated furnace [12], following the schedule reported in Table 3. In the following discussion, samples labeled as LO#LOx#C-16 were sintered at 1600 °C for 24 h, whereas samples labeled as LaO#LaOx#C-18 were sintered at 1600 °C for 24 h and then at 1800 °C for 9 h. Samples sintered at the same final temperature (1600 and 1800 °C, as reported) were heat treated in one batch.

Table 1
Overview of the prepared samples

Sample	La_2O_3 (wt%)	$La_2(C_2O_4)_3$ (wt%)	Graphite (wt%)	$La_2O_3/La_2(C_2O_4)_3$ (molar ratio)
LOC	71.2	–	28.8	1/0
LO7LOx3C	42.7	30.5	26.8	7/3
LO5LOx5C	27.9	46.4	25.7	5/5
LO3LOx7C	15.4	59.8	24.8	3/7
LOxC	–	76.3	23.7	0/1

Table 2
Overview of starting powders

La_2O_3	Aldrich, 99.99%	LO
$La_2(C_2O_4)_3 \cdot 8H_2O$	Aldrich, 99.99%	LOx
Graphite	Aldrich, 99.99% (−325 mesh), (−100 mesh for sample LOC)	C

Table 3
Heat treatments schedule

Heating rate	1st Dwelling	2nd Dwelling	3rd Dwelling	4th Dwelling (sample-18)	Cooling rate
2 °C/min	80 °C, 8 h	1300 °C, 24 h	1600 °C, 24 h	1800 °C, 9 h	2 °C/min

The heat treatment, summarized in Table 3, was designed in order to:

- out-gas the green samples (1st dwelling);
- promote the carbothermal reaction (2nd dwelling);
- sinter the LaC_2-C mixture (3rd and 4th dwelling).

After carburization and sintering, samples were transferred to an inert atmosphere glove box (H_2O and $O_2 < 1$ appm) in order to prevent the reaction of lanthanum dicarbide with moist air.

The morphology and composition of the prepared samples were investigated by means of a Scanning Electron Microscope (Philips XL-30, SEM) equipped with elemental analysis (EDS) probe. Crystalline phases of the samples were studied by means of an X-ray diffractometer (Philips PW 1710, XRD) in Bragg-Brentano configuration using a Cu Kα radiation. Mercury Intrusion Porosimetry (MIP, Pascal 240 Porosimeter) was performed on a selected number of samples in order to measure the amount of open porosity in the samples. Pycnometry measurements under He flow, performed on ground samples with the same composition as for MIP measurements, allowed to obtain the true sample density (ρ_{tm}), and consequently to calculate the amount of closed porosity. The measured true density was compared to the theoretical value (ρ_{tc} in the following) calculated taking into account the stoichiometric ratios for LaC_2 and C, as derived from Eq. (3), as the weighted average of the densities of bulk LaC_2 (5.02 g/cm^3, Espimetals MSDS) and graphite (1.90 g/cm^3, Aldrich MSDS) [9]. The bulk density (ρ_{bulk})

was measured as the mass to volume ratio for at least three samples which had the same starting composition. Emissivity measurements were performed by means of a double frequency pyrometer (IRCON) working in the infrared region, as reported in [12].

3. Results and discussion

3.1. Vacuum levels during the heat treatments

In Fig. 1, the pressure in the heating chamber as a function of the heating power (or T) is plotted for samples sintered at 1600 °C and 1800 °C. In the range 25–700 °C, four distinct regions can be detected in the plots. In the first region (pressure levels ranging from 10^{-3} to 10^{-4} Pa) only dehydration/degassing processes occur [11]. On the basis of already reported thermogravimetric studies [9,11], the peaks of the second region (II) can be associated to CO_2 and CO evolutions, while those of regions III and IV can be associated to CO_2 evolution. Carburization and CO evolution starts at about 1000 °C ($p = 7 \times 10^{-4}$ Pa) and reaches its maximum at 1300 °C ($p = 1.2 \times 10^{-2}$ Pa). The sharp decrease in pressure levels at 1300 °C can be associated to the 24 h plateau at this temperature, during which no further gas evolution occurs.

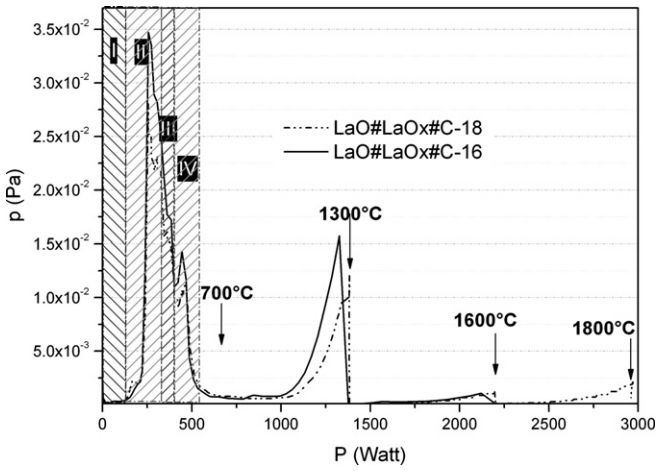

Fig. 1. Vacuum levels upon carburization and sintering.

Table 4
Weight losses and densities after carburization and sintering

Sample	Δwt%	Δwt_{th}%	ρ_{tc} (g cm^{-3})	ρ_{tm} (g cm^{-3})	ρ_{bulk} (g cm^{-3})
LOC-16	18.92 ± 0.02	18.6	4.62	4.74 ± 0.07	3.12 ± 0.06
LO7LOx3C-16	27.64 ± 0.03	27.9	4.54	–	2.25 ± 0.05
LO5LOx5C-16	30.01 ± 0.04	32.9	4.49	4.1 ± 0.04	2.07 ± 0.04
LO3LOx7C-16	38.15 ± 0.05	37.1	4.45	–	1.63 ± 0.03
LOxC-16	43.14 ± 0.05	42.3	4.38	3.91 ± 0.11	1.41 ± 0.03
LO7LOx3C-18	37.73 ± 0.04	27.9	–	–	1.81 ± 0.04
LO5LOx5C-18	43.93 ± 0.05	37.1	–	–	1.60 ± 0.03
LO3LOx7C-18	47.32 ± 0.06	42.3	–	–	1.52 ± 0.03

The heating up to 1600 °C led to further gas evolution (CO), which, at least in part, can be attributed to the completion of the carburization reaction on the pellets top which, as revealed by a calibration experiment, is about 150 °C colder than the bottom (which is directly in contact with the graphite heating element). It is also worth considering that, at these temperatures, some gas release could derive from the experimental equipment itself. The decrease in pressure levels can again be associated with the 24 h plateau, corresponding to the sample sintering. In the experiments continued up to 1800 °C, some unexpected gas release was observed after the completion of the carburization process. The weight losses (see Table 4) are higher than expected for samples sintered up to 1800 °C. Moreover, SEM-EDS investigations on two samples with the same starting composition (LaO5LaOX5 C) treated at 1600 °C and at 1800 °C show an almost complete disappearance of lanthanum dicarbide from the surfaces of the pellets treated at 1800 °C (Fig. 2).

A comparison of the SEM images of the top and bottom surfaces of the same sample treated at 1800 °C (Fig. 3), shows the non-negligible effect of the temperature gradient on the sample composition.

Thus, the higher weight loss and the absence of bright grains of lanthanum dicarbide in the samples treated at 1800 °C may be attributed to an extensive sublimation of lanthanum dicarbide from the samples at pressures of the order of 10^{-4} Pa. Considering that the pyrometer readings reflect the status of the top surface of the samples and that the surface of the samples in contact with the crucible has temperatures about 150 °C higher than those of the top surface, this observation is in good agreement with previously reported literature results [13] which show that the vapor pressure of pure LaC_2 follows the relationship $\log P_{LaC2}\,(\mathrm{Pa}) = (-3.327 \times 10^4/T) + 12.813$ in the temperature range 1327–2327 °C, thus leading to a sublimation temperature of 1705 °C at the pressure of 1×10^{-4} Pa.

3.2. Effect of the $La_2O_3/La_2(C_2O_4)_3$ ratio in the starting mixtures on the porosity of carburization products

In Table 4, an overview of weight variations after carburization and sintering compared with calculated values is reported. The

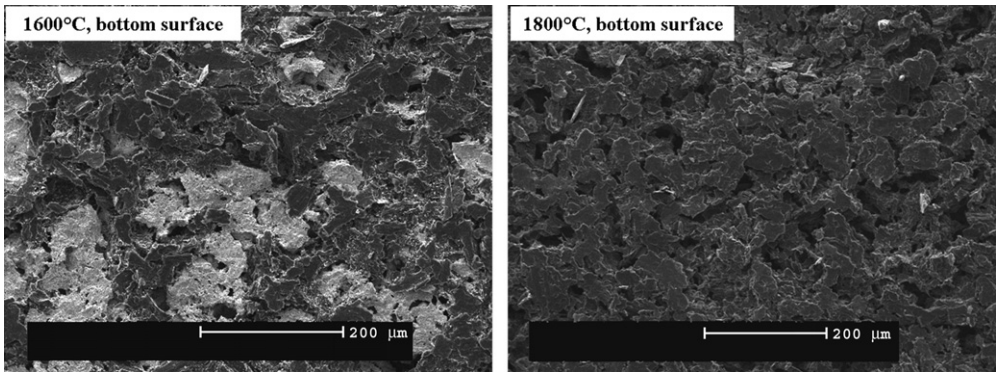

Fig. 2. SEM micrographs with the same magnification of the samples LaO5LaOx5C treated at different temperatures; on the left the upper temperature was 1600 °C, on the right the upper temperature was 1800 °C. The images were collected from the same surface side (bottom surface, in contact with the crucible). The sample heated at 1800 °C does not reveal the presence of the bright grains of lanthanum carbide.

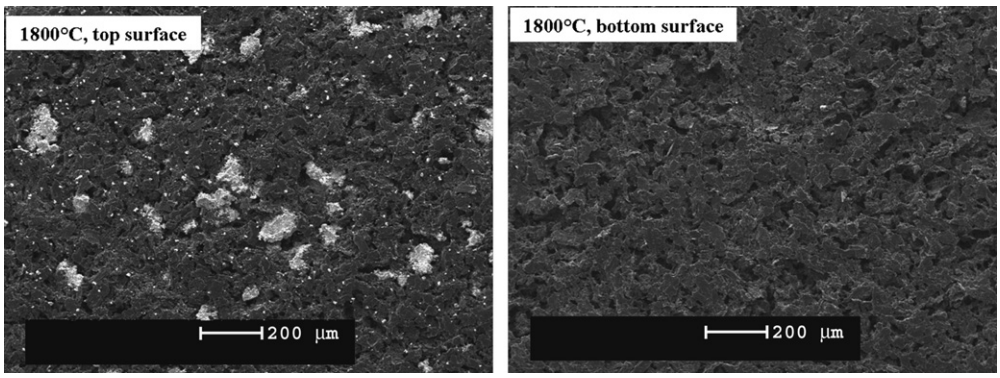

Fig. 3. SEM micrographs at the same magnification of the sample LaO5LaOx5C treated at 1800 °C, collected from the different sample sides. The bottom surface (side down) does not display the presence of bright grains.

data reported in Table 4 show a good agreement between calculated and observed values for samples sintered at 1600 °C. The general trend shows an observed weight loss 0.5–2 wt% higher than the calculated one. This can be attributed to the decomposition of the binder added in excess to the starting mixtures during pellets preparation. Only sample LO5LOX5C-16 deviates from the trend: observed values are almost 3% lower than those calculated. Samples sintered at 1600 °C and then heated to 1800 °C revealed a weight loss higher than expected. This behavior, as previously observed, can be associated to a partial sublimation of LaC_2 at the highest temperatures.

In Table 4, the calculated theoretical density (ρ_{tc}) is reported and the values are compared to the true density measured by He-pycnometry after grinding (ρ_{tm}). Both in calculated and measured values, the true density tends to decrease with increasing amount of $La_2(C_2O_4)_3$ in the starting mixture. This can certainly be attributed to the increased amount of graphite in the final composition of the materials prepared with starting mixtures which are richer in lanthanum oxalate (see Eq. (4)). However, the measured true density (ρ_{tm}) shows a more remarkable decrease compared to the calculated values. This behavior may be correlated to the presence of a certain degree of closed porosity, still present after grinding the samples for the pycnometry analysis. The open porosity (P_{open}) values, obtained by MIP, indeed confirmed these results. The total porosity can be expressed as the sum of closed and open porosity, according to Eqs. (6) and (7)

$$P_{tot} = P_{close} + P_{open}, \quad (6)$$

$$P_{tot} = 1 - \rho_{bulk}/\rho_{tc}, \quad (7)$$

where P_{close} is the closed porosity, P_{open} is the open porosity, ρ_{bulk} is the apparent density and ρ_{tc} is the theoretical density calculated from the stoichiometric amounts of LaC_2 and C (Eq. (3)) as weighed average of their densities (5.02 g/cm^3 and 1.9 g/cm^3, respectively).

In Fig. 4 is reported the effect of increasing percentages of lanthanum oxalate in the starting mixtures on the porosity of final materials after sintering at 1600 °C. Both P_{tot} and measured P_{open} are plotted. P_{tot} was calculated from Eq. (7) using the theoretical ρ_{tc} values reported in Table 4. In the sample LOC-16 the total porosity value approaches that one of open porosity, thus evidencing an almost complete absence of closed porosity. As the content of oxalate increases a remarkable increase in both total and open porosity is clearly observed, thereby proving that the presence of lanthanum oxalate in the reaction mixture effectively introduces a considerable amount of porosity. Although the amount of introduced interconnected open pores is predominant, a non-negligible amount of closed porosity is also present in the heat treated oxalate containing samples, as demonstrated by the difference between total porosity and open porosity values. Even though the mechanism is not clear yet and still under consideration, the $La_2(C_2O_4)_3$ may be considered responsible for the formation of closed porosity upon carburization and sintering. The open porosity increases with increasing the amount of lanthanum oxalate in the starting mixture, with a maximum of 61.6% for sample LOxC-16 (100 wt% $La_2(C_2O_4)_3$) and a minimum of 34.2% for sample LOC-16 (100 wt% La_2O_3). At the same time, the introduction of $La_2(C_2O_4)_3$ gives rise to closed porosity formation even though in a small quantity compared to the total porosity (i.e. for sample LOxC-16 the ratio $P_{close}/P_{tot} = 0.23$).

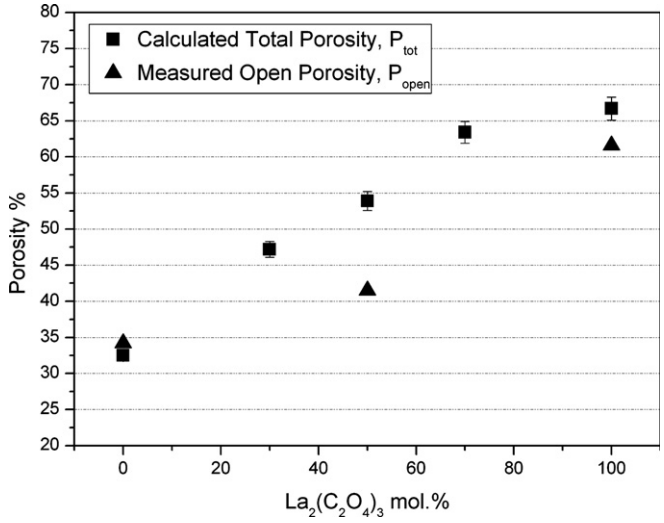

Fig. 4. Effect of the molar amount of Lanthanum oxalate on total porosity and open porosity, for samples sintered at 1600 °C.

The cumulative pore size distribution, obtained by MIP, revealed the presence of pores with size ranging from 0.8 μm, for sample LaOC-16, to 1.3 μm, for sample LaOxC-16. Moreover, the sample LaOC-16 revealed a broader pore size distribution than that observed for the samples prepared with oxide/oxalate mixtures.

In Fig. 5, SEM micrographs of the bottom surfaces of the samples treated at 1600 °C are shown. A remarkable porosity increase is evident by comparing the surface of the sample obtained by treating the sample containing only lanthanum oxide in the starting composition with that containing equal amounts (in moles) of oxide and oxalate. Finer morphological changes can be observed in the samples with intermediate composition.

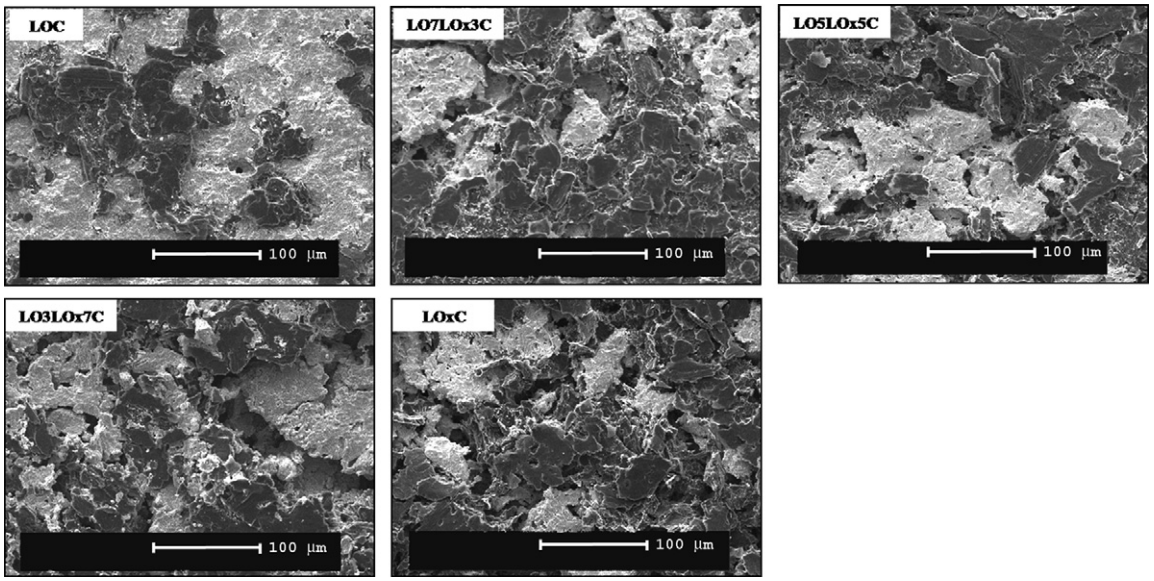

Fig. 5. SEM micrographs (same magnification) of the bottom surface of the samples treated at 1600 °C, with different starting composition of lanthanum oxide/oxalate.

3.3. Effect of the sintering temperature on the composition and sintering degree of the samples

XRD patterns were collected on ground samples. Powders were protected from moisture by sealing them with 25 μm film of Saran™ (trademark for polyvinylidene dichloride). The use of a film of Saran had however the negative side effect of giving noisier diffraction patterns and the appearance of a broad peak at 31.2°, overlapping the secondary peak of LaC_2.

In Fig. 6, the diffraction pattern of the sample LO7LaOx3C-16 is reported as an example. A comparison between the diffraction patterns of LO3LOx7C-16 and LO3LOx7C-18 did not reveal any appreciable difference among their crystalline phases. In both samples, tetragonal LaC_2 and hexagonal graphite were detected, thus pointing out that the carburization successfully occurred also with lanthanum oxalate as reactant for the carbothermal process. Owing to the noise due to the Saran™ layer, a quantitative analysis of the patterns could not be performed.

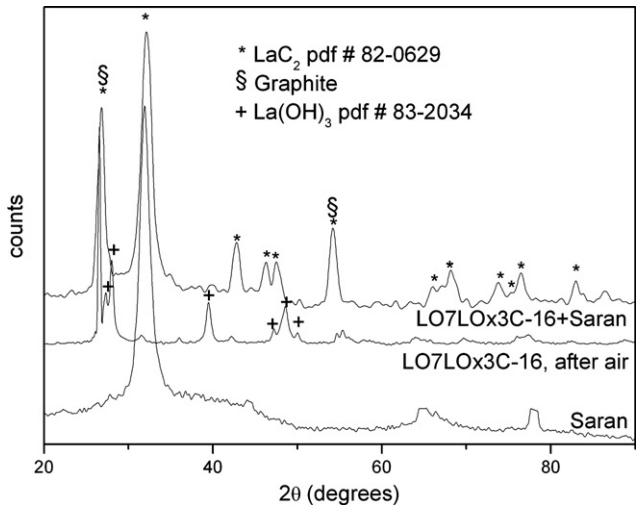

Fig. 6. Diffraction patterns of the sample LO3LOx7C-16 after sintering. Upper, the diffraction pattern of the sample protected by Saran; lower, the diffraction pattern of unprotected sample after 1 h of air exposure.

In Fig. 7 the SEM micrographs of the bottom side of two samples [LOC-16 (100% oxide) and LOxC-16 (100% oxalate)] collected at the same magnification are reported with the corresponding EDS spectra of the bright and black features. It is worth noting that the XRD patterns of the ground samples did not contain any peaks attributable to crystalline phases of compounds containing oxygen. The presence of oxygen is, instead, clearly observable in the EDS spectra of the surfaces of the samples. This dishomogeneous result can be explained as a consequence of the formation of a thin layer of lanthanum hydroxide, which, in spite of the careful procedures adopted to protect samples, formed anyhow by reaction of moist air with the outer lanthanum dicarbide grains. This discrepancy between EDS and XRD results has been already noted and similarly explained in [9].

In order to further verify this hypothesis, further experiments were performed. In Fig. 6 are shown the diffraction patterns of the sample 7LO3LOxC-16 protected by Saran™ and unprotected (1 h of air exposure). The clear evidence of the formation of $La(OH)_3$ in the air-exposed sample reflects the high reactivity of LaC_2 towards water in this material. A similar experiment was performed on a sample prepared with a starting mixture containing only lanthanum oxalate and graphite (LOxC), treated at 1600 °C. After SEM-EDS analysis, the sample was exposed to ambient air for 1 h. During this time, a strong and pungent smell was emitted from the sample which, after subsequent analysis, showed dramatic changes in the surface morphology. Fig. 8 shows that the regularly shaped grains of lanthanum dicarbide, characteristic of the protected sample, have converted into particles with sharp edges, surrounded by large voids, after air exposure. Comparison of EDS analyses reveals the effective decrease of carbon content and increase of oxygen in the surface of the samples after air exposure. This is in agreement with the hydrolysis reaction which, as proposed by Greenwood [14], occurs giving mainly acetylene, hydrogen and lanthanum hydroxide.

3.4. Emissivity

Emissivity values measured during carburization and sintering of samples LaOC-16, LaO7LaOx3C-16 and LaOxC-16 are reported in Fig. 9. Carburization, and consequent CO release, affects mainly the emissivity of the sample prepared starting from the oxide/

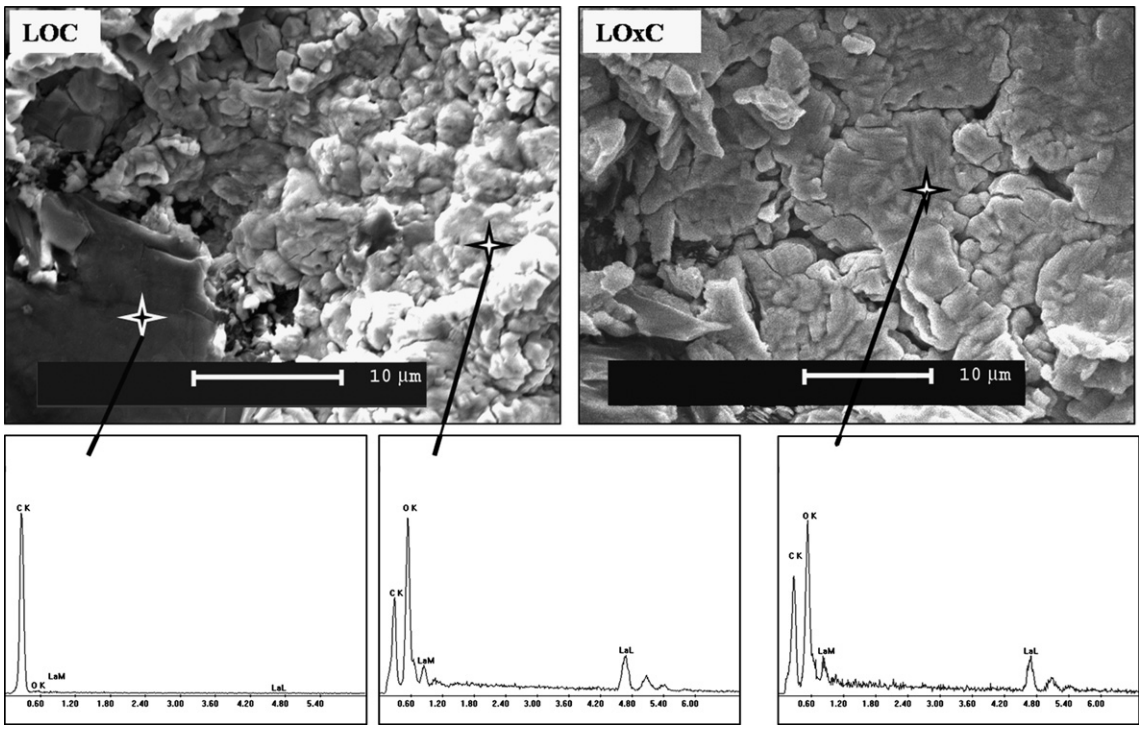

Fig. 7. SEM micrographs collected from the bottom surface of samples LOC and LOxC and EDS analysis on the bright grains and black grains.

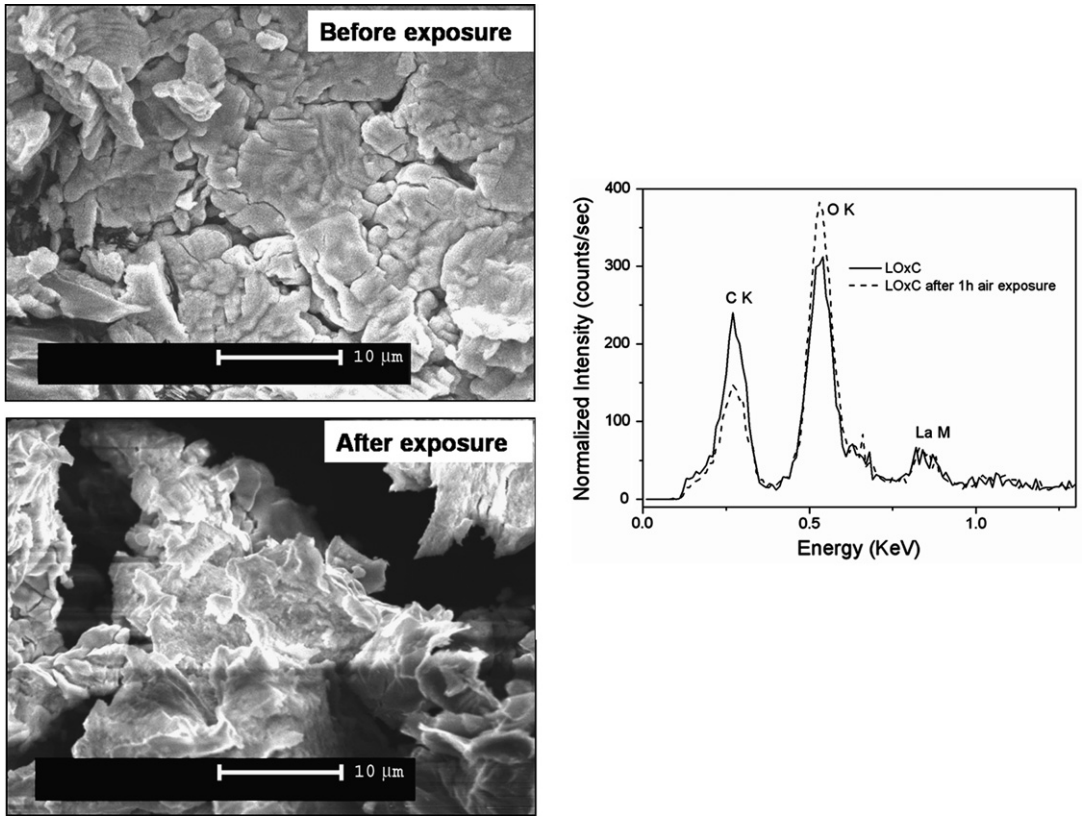

Fig. 8. Surface morphology (same magnification) and EDS analyses of the sample LOxC treated at 1600 °C, before and after exposure to ambient air for 1 h.

oxalate mixture. In fact, the plots in Fig. 9 show that: (a) a sudden decrease of the emissivity characterizes the carbothermal reduction of LaO7LaOx3C-16; (b) the emissivity decrease of the sample prepared starting with a mixture formed only by lanthanum oxide and graphite is less abrupt and more limited; (c) the emissivity of the sample prepared starting from $La_2(C_2O_4)_3$ and graphite follows

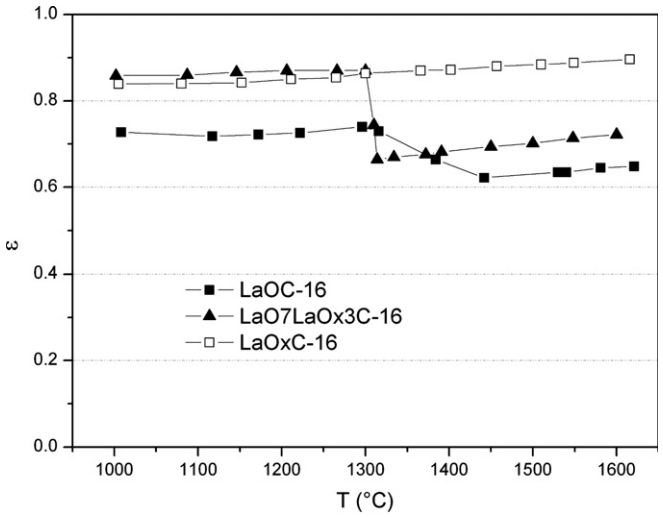

Fig. 9. Emissivity values measured during the carbothermal reduction and sintering of samples LOC-16, 7LO3LOxC-16 and LOxC-16.

a completely different path: it linearly increases with temperature and apparently it is not affected by CO release.

This behavior can be explained as a consequence of the changes of the porosity of the materials due to the carbothermal reduction. Fig. 9 shows that almost at any temperature (with a small exception during carbothermal reduction) the emissivity of the sample prepared starting from La_2O_3 and graphite (LaOC-16) presents always lower values of emissivity compared to those of the samples LaOxC-16 and LaO7LaOx3C-16. As reported by Progelhof et al. [15], the absorbance and consequently the emittance of a porous surface may be related to its porosity (fractional volume) and to the emissivity of its pores, which act as a blackbody, according to Eq. (8)

$$\varepsilon = \varepsilon_0(1-\phi) + \varepsilon_p\phi, \tag{8}$$

where

ε is the emittance of the porous body,
ε_0 is the emittance of non-porous material,
ε_p is the emittance of the pores ($\varepsilon_p = 1$),
φ is the volume pore fraction.

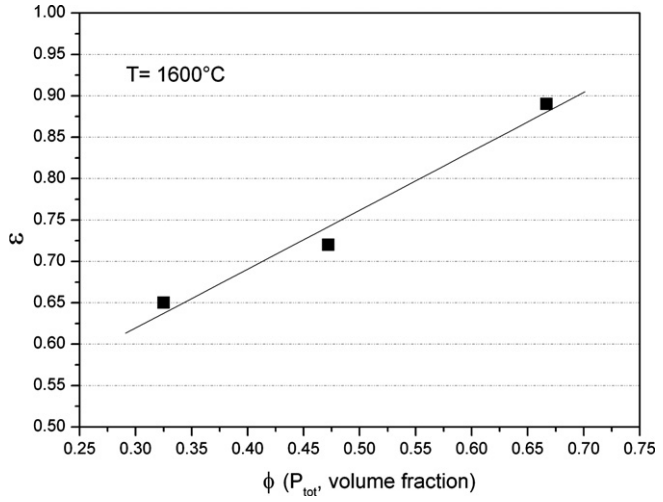

Fig. 10. Emissivity – porosity (volume fraction) relationship at $T = 1600$ °C. The volume fraction of porosity was calculated from Eq. (7).

Moreover, emissivity is a property of the material itself, while emittance is the emissivity of an object with a specific composition, shape, surface finishing, etc.

According to Eq. (8), the emittance of a porous body should lay between the emissivity of the non-porous material and the emissivity of the blackbody ($\varepsilon_0 < \varepsilon < 1$), and increase linearly with the amount of porosity.

In Fig. 10 is shown the relationship existing between the emissivity of the samples (measured after their carbothermal reduction) and their total porosities, for $T = 1600$ °C. A linear increase with porosity percentage is observed, in very good agreement with Eq. (8). Reasonably, as suggested in [14], some corrections to the emittances of the pores as a function of their size and shape, may improve the model. The introduction of $La_2(C_2O_4)_3$ in the starting mixture, thus increased at the same time porosity and emissivity. The increase of both parameters is aimed to the design and production of a target material with improved efficiency.

4. Conclusions

Porous samples of lanthanum dicarbide dispersed in graphite were prepared by carbothermal reduction of samples containing La_2O_3, $La_2(C_2O_4)_3$ or their mixtures, in the presence of excess graphite. The porosity and the bulk density of the samples were controlled by varying the molar ratios among the starting mixtures components (La_2O_3, $La_2(C_2O_4)_3$, C). Total porosity values of the pellets ranged from 32.5 to 66.7 vol.% and the bulk density varied from 3.12 to 1.46 g/cm^3. Substitution of lanthanum oxide with lanthanum oxalate in the starting mixtures increased both the open and, in lesser amount, the closed porosity of the final products. The pore size of the samples, as measured by Mercury Intrusion Porosimetry, was in the range 0.8–1.3 μm. The emissivity measurements of the materials during the entire cycle of carbothermal reduction and sintering (1000–1600 °C) confirmed that a linear correlation exists between the sample emissivity and its porosity, thereby pointing out that the sample emissivity can be tailored through the controlled introduction of porosity. As a matter of fact, the generation of radioactive ion beams with high intensity is an ambitious aim, which must cope as a first step with the complex process of diffusion from the interior of the target. Since the diffusion coefficient in a solid depends exponentially on the operational temperature of the target, it is advisable the use of refractory materials with very high-limiting temperature, such as carbides. However, the choice of high-limiting temperature materials cannot be regarded as the unique approach for the RIB intensity improvement. Great efforts are currently aimed at the synthesis of target materials characterized by high permeability, owing to the fact that in such materials a swift diffusion of the short-lived particles is promoted by the shortened diffusion path. Hence, the results of this study will be employed in the next future in order to improve the overall performance of the targets for the SPES radioactive ion beam facility, by controlling their porosity, density and emissivity.

Acknowledgments

Authors wish to thank Dr I. Nardini and Prof. E. Zendri of the University 'Ca' Foscari' of Venice for MIP measurements and kind assistance.

References

[1] G.D. Alton, J.R. Beene, Y. Liu, Nucl. Instrum. and Meth. A 438 (1999) 190.
[2] A. Andrighetto, S. Cevolani, C. Petrovich, Eur. Phys. J. A 25 (2005) 41.
[3] A. Andrighetto, S. Cevolani, C. PetrovichM. Santana, Eur. Phys. J. A 30 (2006) 591.
[4] C. Lau et al., Nucl. Instrum. and Meth. B 204 (2003) 246.
[5] Y. Zhang, G.D. Alton, Nucl. Instrum. and Meth. A 521 (2004) 72.

[6] H.L. Ravn, T. Bjornstad, P. Hoff, O.C. Jonsson, E. Kugler, S. Sundell, B. VosickiIsolde coll., Isolde coll. Nucl. Instrum. and Meth. B 26 (1987) 183.
[7] J.P. Greene, T. Burtseva, J. Neubauer, J.A. Nolen, A.C.C. Villari, I.C. Gomes, Nucl. Instrum. and Meth. B. 241 (2005) 986.
[8] Y. Kawai, G.D. Alton, J.C. Bilheux, NIM B 241 (2005) 991.
[9] S. Carturan, M. Tonezzer, L. Piga, P. Zanonato, P. Colombo, A. Andrighetto, L. Biasetto, P. DiBernardo, G. Maggioni, F. Gramegna, G. Prete, Nucl. Instrum. and Meth. A 583 (2007) 256.
[10] P Bricault, M. Dombsky, J. Lassen, F. Ames, Triumf Internal PrePrint, TRI-PP-07-31, November 2007.
[11] G. Vanhoyland, R. Nouwen, M.K. Van Bael, J. Yperman, J. Mullens, L.C. Van Poucke, Thermochim. Acta 354 (2000) 145.
[12] L Biasetto, M. Manzolaro, A. Andrighetto, Eur. Phys. J. A, in press.
[13] C.A. Stearns, F.J. Kohl, J. Chem. Phys. 54 (1971) 5180.
[14] N.N. Greenwood, A.J. Osborn, J. Chem. Soc. (1961) 1775.
[15] C.G. Progelhof, J.L. Throne, Effect of surface porosity on emittance of an opaque substance, J. Am. Ceram. Soc. 52 (1969) 227.